

## 3D-QSAR Studies on Angiotensin-Converting Enzyme (ACE) Inhibitors: a Molecular Design in Hypertensive Agents

Amor A. San Juan and Seung Joo Cho\*

Biochemicals Research Center, Korea Institute of Science and Technology, P.O. Box 131, Cheongryang, Seoul 130-650, Korea

\*E-mail: chosj@kist.re.kr

Received February 24, 2005

Angiotensin-converting enzyme (ACE) is known to be primarily responsible for hypertension. Three-dimensional quantitative structure-activity relationship (3D-QSAR) models have been constructed using the comparative molecular field analysis (CoMFA) and comparative molecular similarity indices analysis (CoMSIA) for a series of 28 ACE inhibitors. The availability of ACE crystal structure (1UZP) provided the plausible biological orientation of inhibitors to ACE active site (C-domain). Alignment for CoMFA obtained by docking ligands to 1UZP protein using FlexX program showed better statistical model as compared to superposition of corresponding atoms. The statistical parameters indicate reasonable models for both CoMFA ( $q^2 = 0.530$ ,  $r^2 = 0.998$ ) and CoMSIA ( $q^2 = 0.518$ ,  $r^2 = 0.990$ ). The 3D-QSAR analyses provide valuable information for the design of ACE inhibitors with potent activity towards C-domain of ACE. The group substitutions involving the phenyl ring and carbon chain at the propionyl and sulfonyl moieties of captopril are essential for better activity against ACE.

**Key Words :** 3D-QSAR, Angiotensin-converting enzyme, CoMFA, CoMSIA, Hypertension

### Introduction

Angiotensin-converting enzyme (ACE) is involved<sup>1</sup> in hypertension, heart failure, myocardial infarction and diabetic nephropathy. Angiotensin is a vasoconstrictive peptide that directly influences the pathophysiology of coronary artery disease with pivotal role in blood pressure regulation. ACE is a metalloprotease catalyzing<sup>2</sup> the hydrolysis of carboxy-terminal dipeptides from oligopeptide substrates. Previous ACE inhibitors including captopril, lisinopril and enalapril were developed on the basis of an assumed mechanistic homology with carboxypeptidase-A wherein clinical results<sup>3</sup> showed side effects such as cough and angioedema. The knowledge of the three-dimensional structure<sup>4</sup> of human ACE holds a promise to develop a hypertensive drug with minimal side effects and higher efficacy.

ACE is composed of functionally N- and C- domains that differ in substrate and inhibitor specificity and chloride activation. Both domains have zinc catalytic component located at the active site. The C-domain<sup>3</sup> is primarily responsible for high blood pressure. In contrast to the C-domain, the N-domain seems to have relatively low affinity for the peptides that control blood pressure. The C-domain active site<sup>4</sup> but not the N-domain in ACE is strongly activated by chloride ion. The crystal structure of somatic ACE resembles the testis ACE (*t*ACE). The structure of *t*ACE (Figure 1a) bound to captopril drug reveals<sup>4</sup> the surface cavity of the active site showing the steric and cleft features of protein with color-coded map representing the distribution of positive (blue color) and negative (red color) charges on the macromolecule surface. The stereo representation (Figure 1b) displays the molecular interaction of *t*ACE protein residues in the active site bound to captopril.

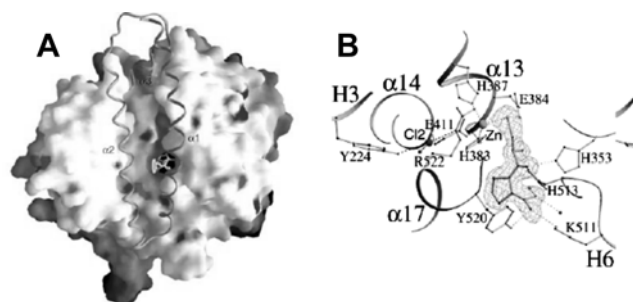


**Figure 1.** The *t*ACE<sup>4</sup> bound to captopril showing the molecular surface (A) and protein residues interatomic interactions (B).

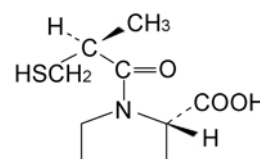


**Figure 2.** The chemical structure of captopril.

The captopril is a specific competitive inhibitor of angiotensin I-converting enzyme that is responsible for the conversion of angiotensin I to angiotensin II. The drug captopril is designated chemically as 1-[(2*S*)-3-mercapto-2-methylpropionyl]-L-proline with the chemical structure shown in Figure 2.

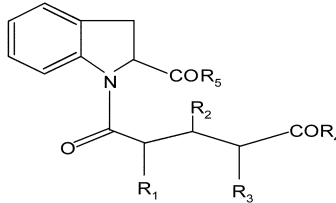
The goal of the study is to design potential ACE inhibitor targeting the C-domain that is expected to show minimal side effects to human. To understand about the steric, electrostatic, hydrophobic and hydrogen bonding properties of ACE inhibitors, we performed three-dimensional quantitative structure activity relationship (3D-QSAR) to series of 1-glutarylindoline-2-carboxylic acid compounds<sup>5</sup> as well as

carboxyalkanoyl and merkptoalkanoyl amino acid derivatives.<sup>6</sup> Both of the 3D-QSAR techniques including comparative molecular field analysis (CoMFA) and comparative molecular similarity indices analysis (CoMSIA) were employed to study the interatomic interaction between the ligand (series of ACE inhibitors) and the receptor (*t*ACE). CoMFA analysis calculates<sup>7</sup> both the steric and electrostatic properties of compounds based on Lennard-Jones and Coulomb potentials. For a more detailed structure activity studies, CoMSIA provides<sup>8</sup> similarity indices of compounds by hydrophobic and hydrogen bond donor and acceptor fields. Graphical representations of 3D-QSAR computational results were depicted by contour maps showing the steric, electrostatic, hydrogen bonding and hydrophobic interactions of ligand bound to the receptor.

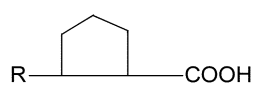
## Methods

The first group of compounds used for the 3D-QSAR analyses includes series of 1-glutarylindoline-2-carboxylic acid (GCA) sourced from CIBA-GEIGY<sup>5</sup> pharmaceuticals. Gruenfeld *et al.* reported<sup>5</sup> the biochemical assay of GCA compounds ACE inhibitors that were tested against hypertensive rat tissue by an oral dose of 30 mg·kg<sup>-1</sup>. The biochemical assay studies<sup>5</sup> contain about 29 compounds with IC<sub>50</sub> values within the range of 4.8 to 290,000 nM (Table 1). Out of the 29 compounds, only 17 compounds (compound 1-17) were chosen based on the criteria of selectivity. The second group of compounds utilized twelve compounds that were drawn from carboxyalkanoyl and merkptoalkanoyl amino acid (CMA) derivatives.<sup>6</sup> The

**Table 1.** The binding affinities of GCA<sup>5</sup> and CMA<sup>6</sup> series of compounds as ACE inhibitors



**GCA**



**CMA**

Compounds	R1	R2	R3	R4	R5	R	IC50 (nM)
1	H	H	H	OH	OH		260
2	Me	H	H	OH	OH		64
3	Me	H	H	OMe	OH		6900
4	Me	H	H	NH <sub>2</sub>	OH		16000
5	(R)-Me	H	H	OH	OH		44
6	(R)-Me	H	H	OEt	OH		11000
7	I-Pr	H	H	OH	OH		50
8	H	Me	H	OH	OH		37000
9	H	Me <sub>2</sub>	H	OH	OH		290000
10	H	H	Me	OH	OEt		920
11	H	H	Me	OH	OEt		170000
12	Me	H	Me	OH	OH		8800
13	Me	H	Me	OH	OH		190
14	Me	H	Me	OH	OH		54
15	(R)-Me	H	(R)-Me	OH	OH		28
16	(R)-Me	H	(R)-Me	OEt	OH		5500
17	(R)-Me	H	(R)-Me	OH	OEt		28000
18						HOOCCH <sub>2</sub> CH(CH <sub>3</sub> )CO	2.2
19						HOOCCH(CH <sub>3</sub> )CH <sub>2</sub> CO	61
20						HOOCCH <sub>2</sub> CH(CH <sub>3</sub> )CO	148
21						HOOCCH(CH <sub>3</sub> )CH <sub>2</sub> CO	260
22						HOOCCH <sub>2</sub> CH <sub>2</sub> CH(CH <sub>3</sub> )CO	0.49
23						HOOCCH <sub>2</sub> CH(CH <sub>3</sub> )CH <sub>2</sub> CO	120
24						HOOCCH(CH <sub>3</sub> )CH <sub>2</sub> CH <sub>2</sub> CO	26
25						HOOCCH <sub>2</sub> CH <sub>2</sub> CH(CH <sub>3</sub> )CO	95
26						HSCH(CH <sub>3</sub> )CO	0.11
27						HSCH <sub>2</sub> CH(CH <sub>3</sub> )CO	0.0023
28						HSCH(CH <sub>3</sub> )CH <sub>2</sub> CO	0.11
29						HSCH <sub>2</sub> CH(CH <sub>3</sub> )CO	0.24

CMA derivatives reported by Cushman and co-workers were similarly tested to rat models at pH = 8.9. The similar source of rat models for the GCA and CMA series of compounds is essential as the modeling study is derived from a non-biased input data.

Molecular modeling calculations were performed using SYBYL<sup>9</sup> program version 7.0 on silicon graphics origin300 workstation with IRIX 6.5 operating system. Energy minimizations of compounds were accomplished by assigning Tripos force field<sup>10</sup> and Merck molecular force field 94 (MMFF94) charges with BFGS method at convergence criterion of 0.005 kcal·mol<sup>-1</sup>. The two alignment techniques employed in this study include the atom-fit and docking. In a standard CoMFA procedure, a bioactive conformation is critically chosen to obtain a suitable conformational template of the ligand's 3D structures. Unlike docking alignment, atom-fit requires a bioactive conformer as template in aligning the rest of the compounds in the series. The crystal structure<sup>11</sup> of captopril bound to *t*ACE protein was used as a basis for constructing the bioactive conformation of the combined 29 compounds.

Partial least squares (PLS) methodology was employed for all 3D-QSAR modeling studies. The CoMFA and CoMSIA descriptors were used as independent variables, and the pIC<sub>50</sub> values were utilized as dependent variables in PLS analyses to derive 3D-QSAR models. Initially, the predictive value of the models was determined by leave-one-out (LOO) cross-validation. To maintain the optimum number of PLS components and minimize the tendency to over fit the data, the number of components corresponding to the lowest PRESS value was employed to obtain the final PLS regression models. The 3D-QSAR visualization of results from the best CoMFA and CoMSIA models have been performed using the "StDev\*Coeff" mapping option. The "StDev\*Coeff" is a standard deviation coefficient with default values of 80% favored contribution and 20% disfavored contribution.

## Results and Discussion

The set of 29 compounds were aligned based on two categories: the atom-fit and docking alignment. Out of 29 compounds, compound 18 was removed because it was detected as an outlier due to its non-selectivity with an observed activity<sup>6</sup> not only to ACE but also to bradykinin. In atom-fit alignment, the structure of captopril extracted from IUZF coordinates was used as a basis of alignment that showed relatively poor predictive value of  $q^2 = 0.469$ ,  $r^2 = 0.998$ . Better statistical model was observed through docking alignment of all compounds to IUZF protein with CoMFA standard model ( $q^2 = 0.530$ ,  $r^2 = 0.998$ ) and with CoMSIA combined steric, electrostatic, hydrophobic and hydrogen bond acceptor fields ( $q^2 = 0.518$ ,  $r^2 = 0.990$ ). The compounds were aligned based on the active site of C-domain *t*ACE protein. The superposition of the 28 compounds by docked alignment is shown in Figure 3. Docking-based alignment is guided by the intermolecular

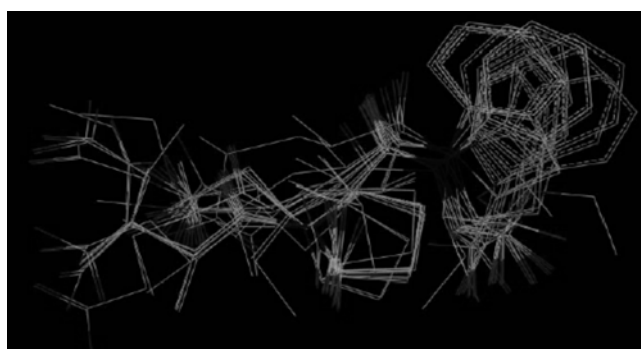


Figure 3. The alignment derived from docking of 28 ACE inhibitors to IUZF protein.

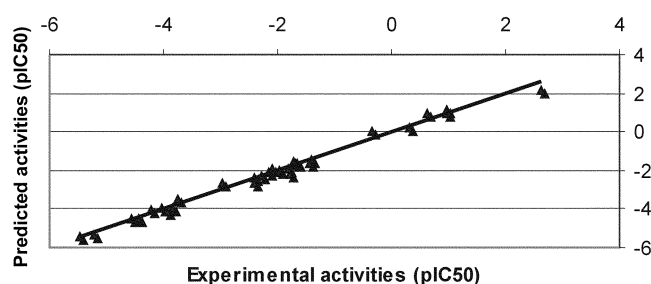


Figure 4. CoMFA predicted versus experimental pIC<sub>50</sub> values ( $r^2 = 0.990$ ).

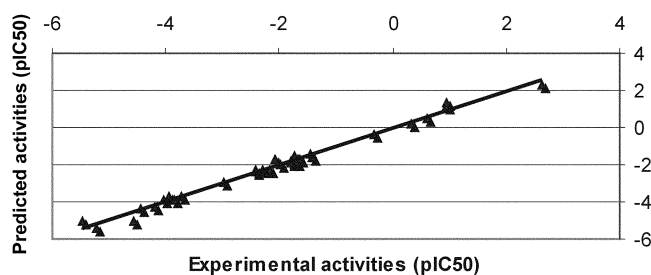


Figure 5. CoMSIA predicted versus experimental pIC<sub>50</sub> values ( $r^2 = 0.989$ ).

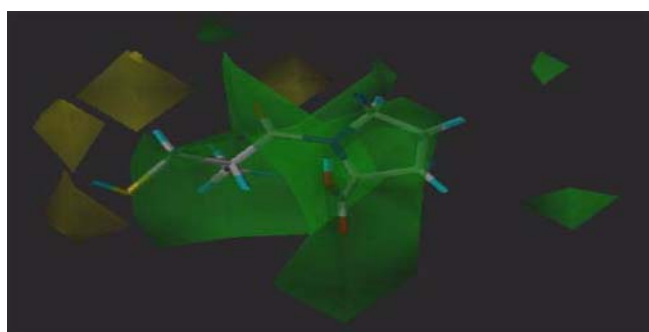
interaction between the ligands and protein hence, provides better alignment as the compounds are superimpose directly into the crystal structure of receptor site.

Figures 4 and 5 show the prediction curves obtained by final CoMFA and CoMSIA 3D-QSAR models. Results showed high correlation between the observed and predicted activities of CoMFA and CoMSIA models. However, FlexX docking energy (see Table 2) of the compounds did not show a general correlation with the pIC<sub>50</sub> that can be attributed to the large structural differences existing among the compounds (Table 1).

In Figure 6 below, the CoMFA steric contour map is shown suggesting that the presence of bulky groups to almost the entire captopril moiety is preferred for an enhanced inhibitor efficacy. Specifically, steric R-groups are favored along the proline ring of the 2-methylpropionyl-L-proline as well as the sulfonyl group of 3-mercapto moieties of the captopril chemical structure (see Figure 2).

**Table 2.** Experimental and predicted activities of CoMFA std and CoMSIA combined models

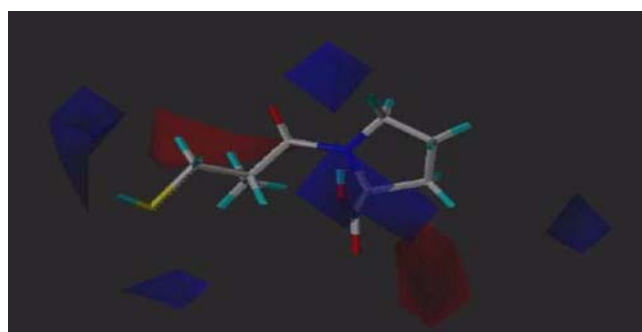
compounds	IC <sub>50</sub> (nM)	Expt'l pIC <sub>50</sub>	FlexX Energy kcal/mol	CoMFA Predicted	CoMSIA Predicted	CoMFA Residuals	CoMSIA Residuals
27	0.002	2.638	-19.700	2.120	2.260	0.520	0.380
26	0.110	0.959	-15.400	1.160	1.190	-0.200	-0.230
28	0.110	0.959	-15.100	0.910	1.350	0.050	-0.390
29	0.240	0.620	-19.500	0.940	0.480	-0.320	0.140
22	0.490	0.310	-23.100	0.230	0.190	0.080	0.120
18	2.200	-0.342	-27.100	0.010	-0.340	-0.350	0.004
24	26	-1.415	-26.300	-1.440	-1.660	0.020	0.240
15	28	-1.447	-23.900	-1.610	-1.430	0.160	-0.020
5	44	-1.643	-21.500	-1.620	-1.680	-0.020	0.040
7	50	-1.699	-23.000	-1.680	-1.940	-0.020	0.240
14	54	-1.732	-20.200	-1.590	-1.530	-0.140	-0.200
19	61	-1.785	-30.200	-2.190	-1.850	0.400	0.060
2	64	-1.806	-24.700	-1.910	-1.900	0.100	0.090
25	95	-1.978	-20.600	-2.010	-1.980	0.030	0.003
23	120	-2.079	-23.100	-1.960	-1.740	-0.120	-0.340
20	148	-2.170	-27.900	-2.110	-2.270	-0.060	0.100
13	190	-2.279	-13.400	-2.330	-2.320	0.050	0.040
1	260	-2.415	-24.800	-2.680	-2.360	0.260	0.060
21	260	-2.415	-28.500	-2.370	-2.310	-0.050	-0.110
10	920	-2.964	-25.000	-2.630	-2.910	-0.330	-0.050
16	5500	-3.740	16.000	-3.540	-3.690	-0.200	-0.050
3	6900	-3.839	-18.400	-3.930	-3.880	0.090	0.040
12	8800	-3.944	-19.000	-4.110	-3.750	0.170	-0.190
6	11000	-4.041	-16.800	-3.970	-3.900	-0.070	-0.140
4	16000	-4.204	-22.100	-4.020	-4.290	-0.180	0.090
17	28000	-4.447	-14.600	-4.510	-4.420	0.060	-0.030
8	37000	-4.568	-24.300	-4.530	-5.000	-0.040	0.430
11	170000	-5.230	-24.400	-5.330	-5.390	0.100	0.160
9	290000	-5.462	-27.100	-5.480	-5.070	0.020	-0.390

\*pIC<sub>50</sub> = -log IC<sub>50</sub>

**Figure 6.** CoMFA steric contour plot (stdev\*coeff as described below). Sterically favored areas (contribution level of 80%) are represented by green polyhedra. Sterically disfavored areas (contribution level 20%) are shown by yellow polyhedra.

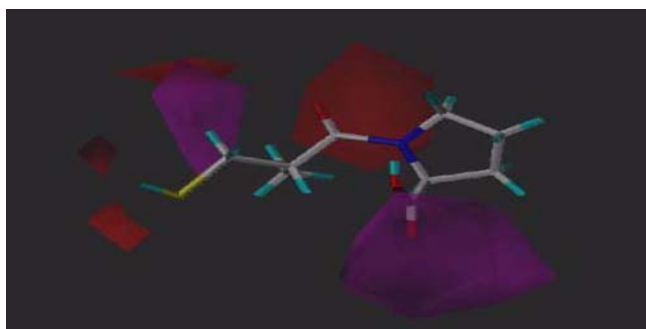
Figure 7 below depicts the CoMFA electrostatic contour map that implies the presence of positive charge group favors the blue color regions located near the propionyl part and similarly at the carboxyl group of the proline moiety of captopril.

Figure 8 below displays the hydrogen bond acceptor



**Figure 7.** CoMFA electrostatic contour plot (stdev\*coeff as described below). Positive charged favored areas (contribution level of 80%) are represented by blue polyhedra. Negative charged disfavored areas (contribution level 20%) are shown by red polyhedra.

contour map of combined CoMSIA (steric, electrostatic, hydrophobic and acceptor fields). The magenta color regions favor hydrogen bond acceptor atoms that is located near the carboxyl group moiety whereas, the red color regions unfavour the hydrogen bond acceptor atoms that is seen near the



**Figure 8.** CoMSIA combined hydrogen bond acceptor contour plot (stdev\*coeff as described below). H-bond acceptor favored areas (contribution level of 80%) are represented by magenta polyhedra. H-bond acceptor disfavored areas (contribution level 20%) are shown by red polyhedra.

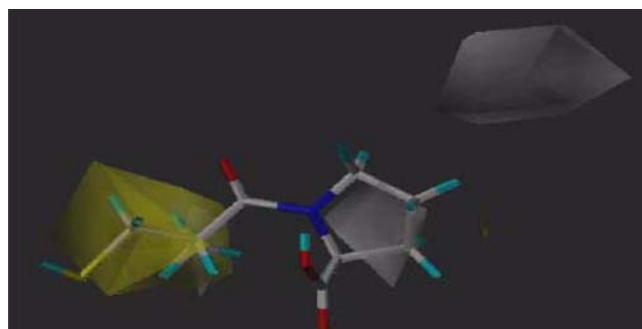


**Figure 9.** CoMSIA combined hydrophobic contour plot (stdev\*coeff as described below). Hydrophobically favored areas (contribution level of 80%) are represented by yellow polyhedra. Hydrophobically disfavored areas (contribution level 20%) are shown by white polyhedra.

carbonyl group as well as in the sulfonyl group.

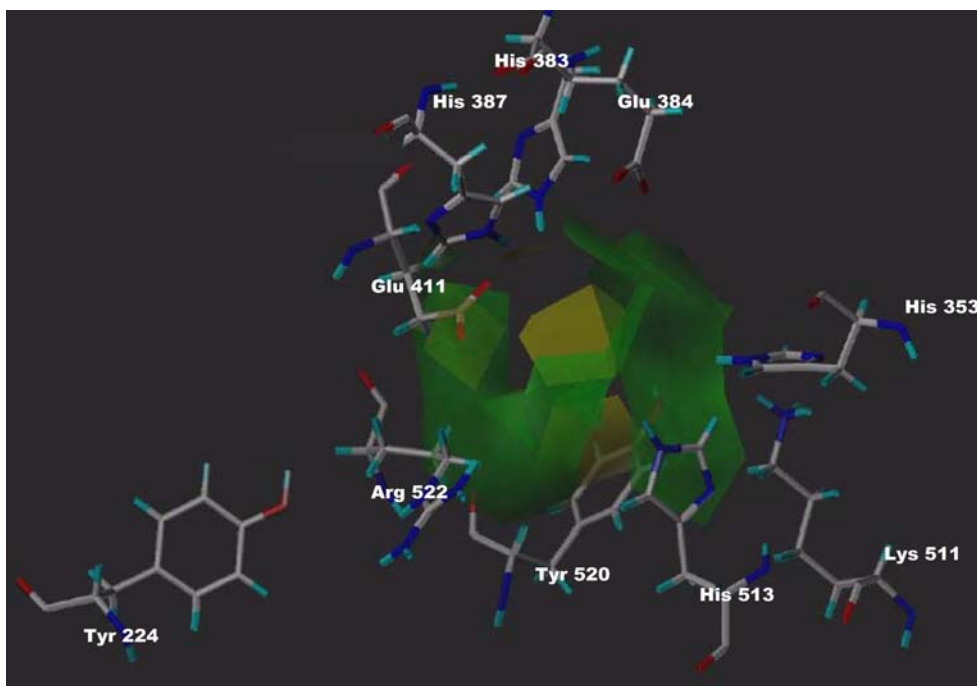
Figure 9 below shows the CoMSIA hydrophobic contour map (on the basis of combined steric, electrostatic, hydrophobic and acceptor fields). The yellow color region at the sulfonyl group suggests that it strongly like to be substituted by a hydrophobic group to have enhanced activity.

Since the crystal structure of *t*ACE was known recently, it was quite interesting to compare the qualitative 3D-QSAR contour maps (both CoMFA and CoMSIA) with the geometrical properties as well as interatomic interactions of the different protein residues located at the active site. An important caution to note is that the “contour coefficient maps” must not be interpreted as the “receptor maps”, as pointed out by the authors<sup>7</sup> of the original CoMFA paper. Despite this fact, when the docking alignment is based on the receptor structure, there is an expectation that degree of

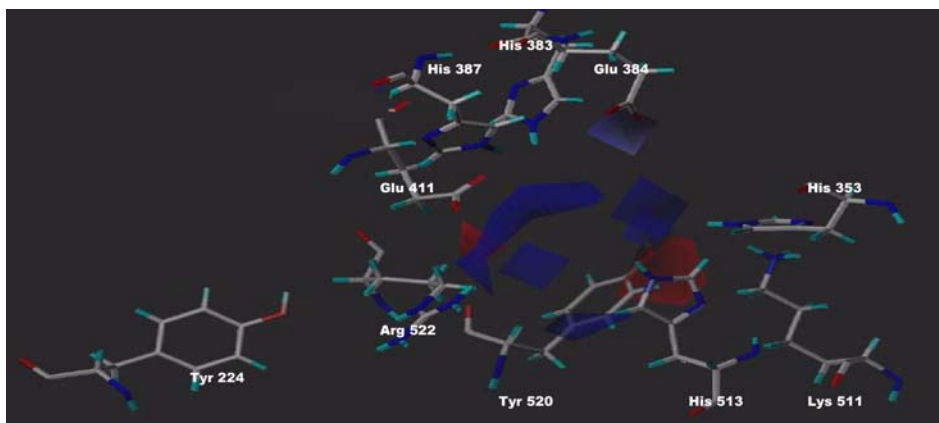
correlation may exist between the contour maps and protein residues in the active site. Thus, we have analyzed the contours shown in Figures 10-13 in relation to the steric, electrostatic, H-bond donor, H-bond acceptor and hydrophobic structural features within the active site.

Figure 10 below depicts the sterically favorable regions (green color) that occupy the cavity in the *t*ACE active site protein residues including His 513, Lys 511, Tyr520, Arg 522 and His 353. On the other hand, the sterically unfavorable regions (yellow color) interact with the protein residues Glu 411, His 387 and His 383. Results show that steric contour maps are consistent with the active site of *t*ACE.

In spite of the correlation between the steric maps and the active site topology, the agreement is less obvious for electrostatic fields, although we do find that the negative



**Figure 10.** Superposition of the CoMFA steric stdev\*coeff contour plot and active site residues.



**Figure 11.** Superposition between the CoMFA electrostatic stdev\*coeff contour plot and active site residues within *t*ACE.

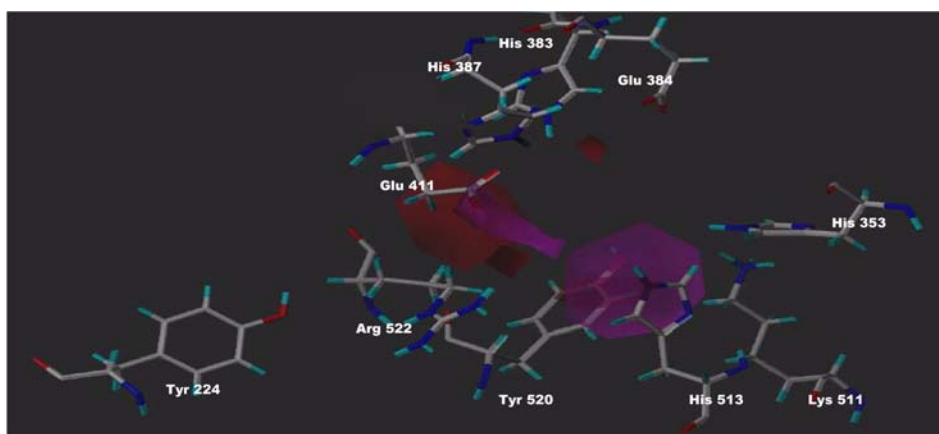


**Figure 12.** Superposition between the CoMSIA H-bond acceptor contour plot (combined) and active site residues within *t*ACE.

charge favorable field (red color, see Figure 11 below) occupies the polar residue His 517. However, the interpretation of positive charge favorable fields seem inconsistent due to the presence of bulky group residues including Tyr 520 and Arg 522 surrounding the blue

contours. Results imply that the degree of output correspondence between CoMFA docking site depends on the chemical structure of the training set.

Further complementary analysis derived from the CoMSIA graphical displays signify correlation with the

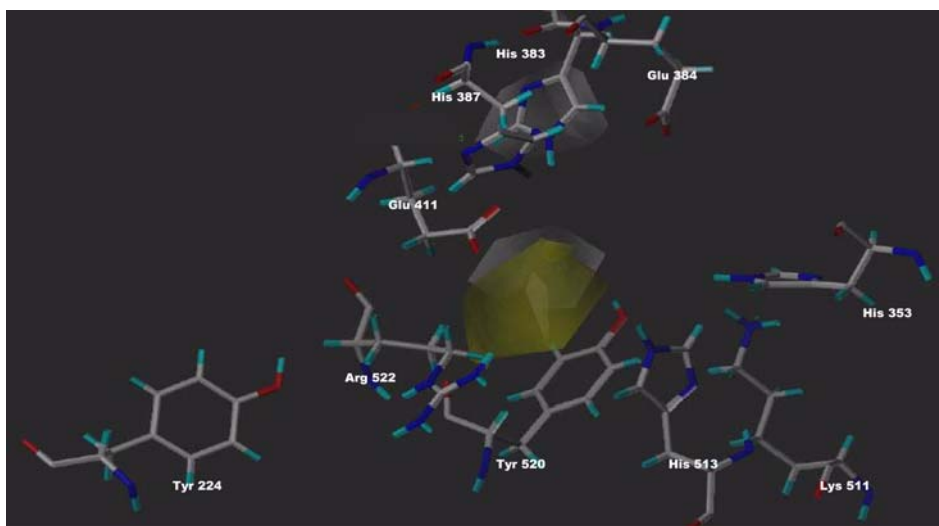


**Figure 13.** Superposition between the CoMSIA hydrophobic contour plot (combined) and active site residues within *t*ACE.

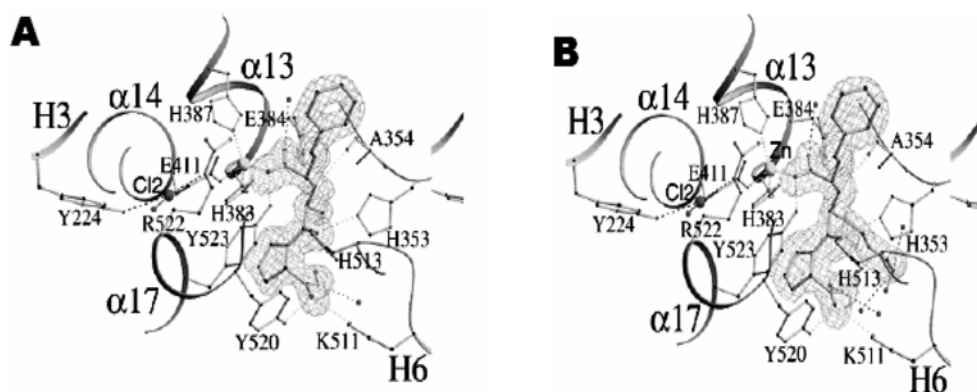


**Figure 14.** The *t*ACE inhibitors<sup>11</sup> with enalapril drug (A) and lisinopril drug (B) located at the center bound to the active site residues.

chemical properties of active site residues. In particular, there is agreement of favorable H-bond acceptor field (Figure 12, magenta color contour) located juxtaposed to electronegative residues Tyr 520, His 517 and Lys 511 that revealed strong hydrogen bonding interaction to captopril (see Figure 1b). The residue Arg 522 that is positioned near the disfavored H-bond acceptor field (Figure 12, red color contour) supports the experimental interaction (Figure 1b) that the chloride ion is stabilized by its molecular interaction to Arg 522 residue.

Future prospects of ACE inhibitors require bulky groups moieties in contrast to small molecule captopril drug. As shown in CoMSIA (combined) hydrophobic contour map below (Figure 13), the white region (favors hydrophobic groups) superposed near the location of protein residues Glu 384 and His 387 suggesting complementary analysis to the second-generation ACE drugs including enalapril and lisinopril. Figure 14 below agrees with our 3D QSAR findings wherein the residues Glu 384 and His 387 in the active site enclosed the bulky hydrophobic groups along the sulfonyl part of enalapril and lisinopril inhibitors.

### Conclusion

The information derived from the model 3D-QSAR graphical displays are useful in molecularly designing new potential drugs against ACE. A compound with steric R-groups along the proline ring and sulfonyl part may enhance the activity towards the C-domain of ACE. Furthermore, the

presence of electropositive group on the propionyl moiety of captopril as well as hydrophobic group at the sulfonyl moiety is expected to increase activity. In general, the analysis of map contours is in correspondence to the steric and electrostatic environment of ACE active site.

### References

1. Dzau, V. J. *J. Hypertens. Suppl.* **1994**, 12(4), S3-10.
2. Ehlers, M.; Riordan, J. *Biochemistry* **1989**, 28(13), 5311-5318.
3. Acharya, R.; Sturrock, E.; Riordan, J.; Ehlers, M. *Nat. Rev. Drug Discov.* **2003**, 2, 891-902.
4. Natesh, R.; Schwager, S.; Sturrock, E.; Acharya, K. *Nature* **2003**, 421, 551-554.
5. Gruenfeld, N.; Stanton, J.; Yuan, A.; Ebetino, F.; Browne, L.; Gude, C.; Huebner, C. *J. Med. Chem.* **1983**, 26, 1277-1282.
6. Cushman, D.; Cheung, H.; Ondetti, M. *Biochemistry* **1977**, 16(25), 5484-5491.
7. (a) Cramer III, R. D.; Patterson, D. E.; Bunce, J. D. *J. Am. Chem. Soc.* **1988**, 110, 5959-5967. (b) Cho, S. J. *Bull. Korean Chem. Soc.* **2003**, 24, 731-732. (c) Bang, S. J.; Cho, S. J. *Bull. Korean Chem. Soc.* **2004**, 25, 1525-1530. (c) Cho, S. J. *Bull. Korean Chem. Soc.* **2005**, 26, 85-90.
8. *3D QSAR Methods*; Klebe, G.; Kubinyi, H.; Folkers, G.; Martin, Y. C., Eds.; Kluwer Academic Publishers: Great Britain, 1998; Vol. 3, p 87.
9. *SYBYL 7.0*; Tripos Inc.: 1699 Hanley Road, St. Louis, MO 63144, 2004.
10. Clark, M.; Cramer, R. III.; Van Opdenbosch, N. *J. Comput. Chem.* **1989**, 10, 982-1012.
11. Natesh, R.; Schwager, S.; Evans, H.; Sturrock, E.; Acharya, K. *Biochemistry* **2004**, 43, 8718-8724.